

Shot timescales in accreting black hole binaries: w spectrum and its application

Hua Feng¹*, Shuang-Nan Zhang^{2,3,4,5} and Ti-Pei Li^{1,2,4}

¹ Department of Engineering Physics and Center for Astrophysics, Tsinghua University, Beijing 100084, China

² Physics Department and Center for Astrophysics, Tsinghua University, Beijing 100084, China

³ Physics Department, University of Alabama in Huntsville, Huntsville, AL 35899, USA

⁴ Laboratory for Particle Astrophysics, Institute of High Energy Physics, Chinese Academy of Sciences, Beijing 100039, China

⁵ Space Science Laboratory, NASA Marshall Space Flight Center, SD50, Huntsville, AL 35812, USA

Abstract We proposed a new statistic w spectrum which can detect the shot width distribution sensitively. By applying the w spectrum to X-ray binaries, we can distinguish between neutron stars and black holes from their different shot behaviours at small timescales. The energy dependent analysis for black hole binaries, in particular for Cyg X-1, can help us to reveal dynamical evidence for black hole accretion flows and state transitions. Both narrow and broad iron $K\alpha$ lines are presented in the w analysis, affording dynamical evidence for iron lines origin.

Key words: methods: data analysis — X-rays: binaries — accretion, accretion disks — stars: individual (Cygnus X-1)

1 INTRODUCTION

Black hole X-ray binaries (for reviews see Tanaka & Lewin 1995; McClintock & Remillard 2004) manifest complex emission variabilities on wide timescales, varying with energies and spectral states. The physics of the accretion flow and state transitions are still unclear in details. A system of timescale analysis on time domain has been established in recent years (Li 2001; Li & Muraki 2002), on basis of which we proposed a new statistics defined as the differential coefficient of the mean absolute difference of a time series (Feng, Li & Zhang 2004) applying to *RXTE* observations of X-ray binaries to study shot emissions resulting in helpful constraints on accretion flow and state transitions (Feng, Zhang & Li 2004).

* E-mail: fenghua01@mails.tsinghua.edu.cn

2 DEFINITION OF THE w SPECTRUM

2.1 Algorithm

Let $\{x(j; \delta t)\}$ denote the originally observed light curve, where $x(j; \delta t)$ (cts/s) is the counting rate during the time interval $[j\delta t, (j+1)\delta t]$ ($j = 0, 1, 2, \dots$), and δt is the time resolution. To study the variability on a larger timescale $\Delta t = M\delta t$, we need to construct a lightcurve with the time step Δt from the original time series by combining its M successive bins as

$$x_m(i; \Delta t) = \frac{1}{M} \sum_{j=iM+m}^{(i+1)M+m-1} x(j; \delta t) \quad \text{cts/s}, \quad (1)$$

where $i = 0, 1, \dots, N-1$ and $m \in [0, M-1]$ is the discrete phase of the time series. The lightcurve $\{x_m(i; \Delta t)\}$ does not include any information about the variation on timescales $\leq \Delta t$. A mean absolute difference of the observed lightcurve at the timescale Δt can be defined as

$$W(\Delta t) = \frac{1}{M} \sum_{m=0}^{M-1} \left(\frac{1}{N-1} \sum_{i=0}^{N-2} \frac{|x_m(i+1; \Delta t) - x_m(i; \Delta t)|}{\Delta t} \right). \quad (2)$$

The $W(\Delta t)$ includes information of variability with timescales larger than or equal to Δt . To extract the information at the timescale Δt , we can calculate the rate of change of $W(\Delta t)$

$$w(\Delta t) = -\frac{dW(\Delta t)}{d\Delta t}. \quad (3)$$

The mean absolute difference for Poissonian background and fluctuation can be derived as

$$W_{\text{noise}}(\Delta t) = \frac{2e^{-2\bar{x}\Delta t} \sum_{n=0}^{\infty} n I_n(2\bar{x}\Delta t)}{\Delta t^2}, \quad w_{\text{noise}}(\Delta t) = -\frac{dW_{\text{noise}}(\Delta t)}{d\Delta t}. \quad (4)$$

with being \bar{x} the average counting rate of the lightcurve and I_n the modified Bessel function of the first kind with the order number n . The signal's value of the statistic w can be derived as

$$w_s(\Delta t) = w(\Delta t) - w_{\text{noise}}(\Delta t). \quad (5)$$

Calculating $w_s(\Delta t)$ by Eq. (5) at different step Δt for an observed lightcurve we can get a timescale spectrum of w_s . The differential coefficients in Eqs. (3) and (4) can be calculated numerically. In practice, a lightcurve may be divided into L segments, we can calculate $w_{s,l}$ for each segment and then obtain the average value and the standard error

$$\bar{w}_s = \sum_{l=0}^{L-1} w_{s,l} / L, \quad \sigma(\bar{w}_s) = \sqrt{\sum_{l=0}^{L-1} (w_{s,l} - \bar{w}_s)^2 / L(L-1)}. \quad (6)$$

2.2 Simulations

Periodic and random shots: In Fig. 1, one time series is periodic shots and the other is randomly distributed shots. A peak around the timescale equal to the shot width appears clearly in either spectrum. The other characteristic timescale, half period, of the periodic series is also shown in its w spectrum with a smaller amplitude. At small timescales, the random shot series has stronger variability than the periodic one, reflected as the larger amplitude in its w spectrum.

Random shots with noise: The w_s spectra of a set of simulated light curves consisting of both white noise and random shots are calculated in Fig. 2. The shot width is randomly sampled from a uniform distribution between $[\tau_1, \tau_2]$ and its profile has either square or Gaussian form. The time resolution is 10 ms and the total duration is 5000 s with each segment of 500 s. The results,

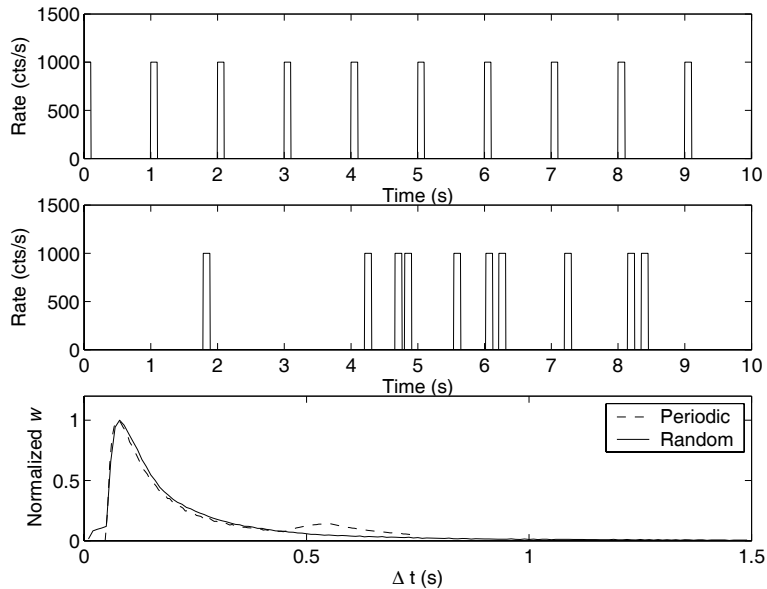


Fig. 1 w spectra for periodic and random square shot series. Top: a periodic square shot series. The square width $t_w = 0.1$ s and the period $T = 1$ s. Middle: a random square shot series. The square width $t_w = 0.1$ s and the interval time between every two neighboring squares follows the exponential distribution with a mean of 1 s. Bottom: w spectra of above series; The time resolution is 5 ms and the total time length is 1250 s with each segment of 250 s.

shown in Fig. 2 (panel (a) for square shots and (b) for Gaussian shots), indicate that we can use the lower timescale cutoff in the w spectrum to measure the shortest width of random shots with high accuracy. For comparison, we also calculate the Fourier power spectrum density (PSD) for each shot series (panel (c) and (d) of Fig. 2 for square and Gaussian shots respectively). It is clear by comparing the PSD with the w_s spectra in Fig. 2 that the w spectrum can be used to detect the shot width more conveniently and accurately.

In sum, the w spectrum is only sensitive to the width distribution of a shot series, but insensitive to shot profile, separation distribution and amplitude. In particular, the w spectrum is especially powerful in detecting the smallest shot width of a shot series.

3 DISTINGUISHING BLACK HOLES AND NEUTRON STARS

The top panel of Fig. 3 shows the normalized w spectra of five black hole binaries (BHBs). All spectra show a cut-off at a timescale about 0.05 s. But for five selected neutron star (NS) binaries with weak magnetic fields, the w spectra have no obvious cut-off above 10^{-2} s (see the bottom panel of Fig. 3). This results is consistent with previous PSD analysis (Sunyaev & Revnivtsev 2000; Li & Muraki 2002).

Furthermore, the energy dependent analysis is carried out for three BHBs at their hard state (Fig. 4). There are three components in a typical plot of shot cutoff timescale vs. energy: (1) descending part at low energies, (2) ascending part at high energies, and (3) a broad iron $K\alpha$ line part around 6 keV. In this observation of GRO J1655–40, the iron line does not appear in timing analysis as well as energy spectrum.

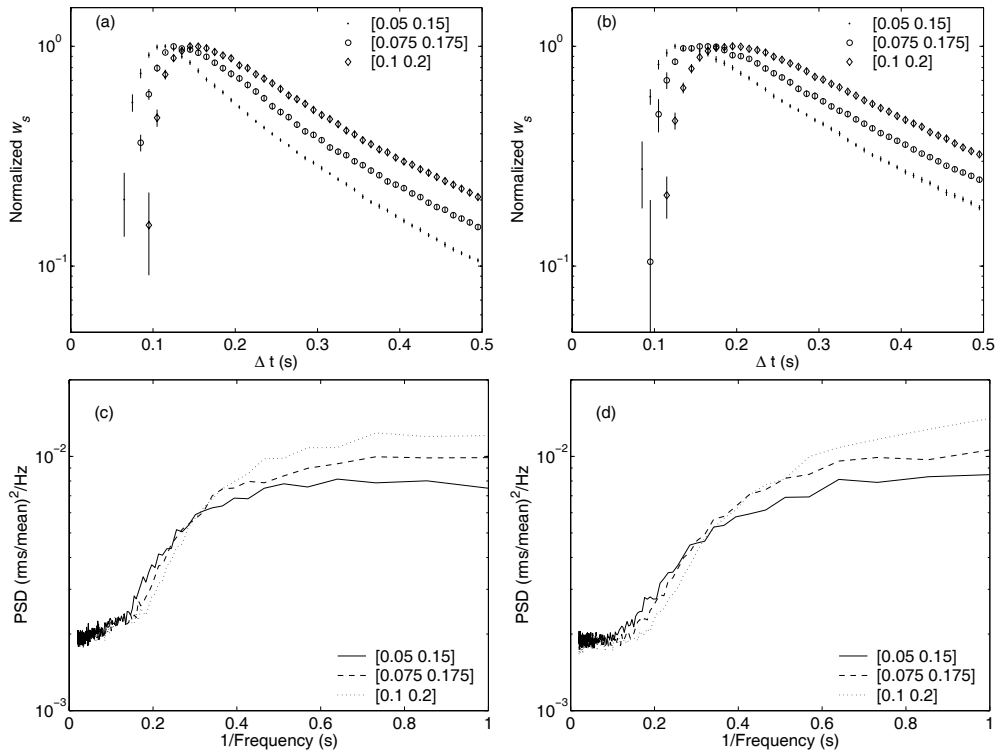


Fig. 2 w spectra for random shots. Shots separations are exponentially distributed with a mean of 1 s. The peak rate of a shot is random from 0 to 1000 cts/s above a background of 1000 cts/s. Poisson counting statistics are included in the simulations. The legend means the timescale regions in which shot width are randomly distributed (width refers to FWHM for Gaussian shots). (a) — w spectra for square shots. (b) — w spectra for Gaussian shots. (c) — PSDs for square shots. (d) — PSDs for Gaussian shots.

In the scope of our discussion, we only consider the shot model as magnetic flares (Poutanen & Fabian 1999), in which the shot timescale is related to the Keplerian timescale, and therefore corresponds to the spatial scale of the accretion flow.

The descending part is possibly originated from emissions in the disk, with higher energy shot located at inner radius causing a decreasing of timescale with increasing energy. The ascending part is related to emissions from the corona; shots are up-Comptonized to increase energy as well as timescale. In this scenario of magnetic flares, The “turning point” (the joint between the descending and ascending parts) is thought to correspond to the innermost region of the accretion disk, where radiations are most variable. The broad peak around 6 keV is caused by the Fe $K\alpha$ fluorescence deduced from the relevant energy spectral analysis.

4 SPECTRAL STATE TRANSITIONS OF CYG X-1

In Fig. 5, the energy dependent shot cutoff timescales in the low, intermediate and high states of Cyg X-1 are presented respectively. It is shown clearly that in the descending part cutoff timescales decrease when the spectral state becomes high/soft. However above the “turning point”, timescales in three states are almost the same.

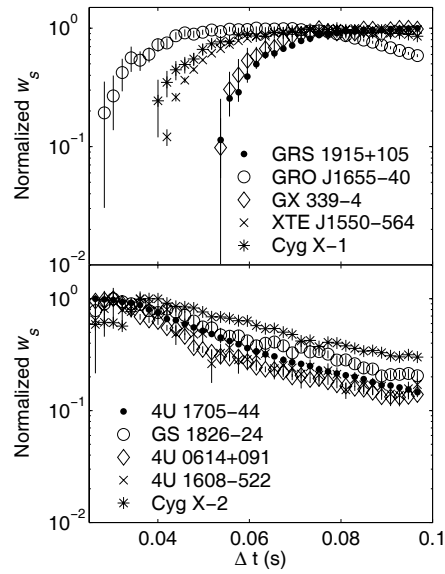


Fig. 3 w spectra for X-ray binaries. Top: black hole binary candidates; Bottom: weakly magnetized neutron star binaries.

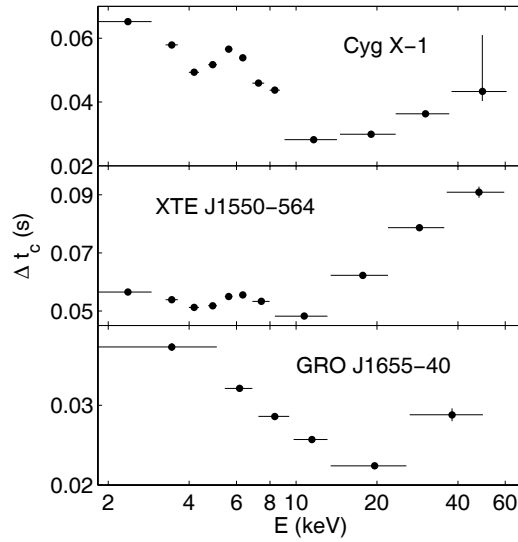


Fig. 4 Shot cutoff timescale versus energy for three BHCs.

To study the inner-state shot timescale evolution as well as the state transitions, power-law spectrum photon indices Γ and shot cutoff timescales τ at different states and different energy bands are shown in Fig. 6. Every energy spectrum is fitted by a multi-color disk model plus a power-law model with a reflection component, i.e., diskbb+pexrav. It is obviously shown that at low energy bands from panels (a) to (g), Γ is inversely proportional to τ . While at energies

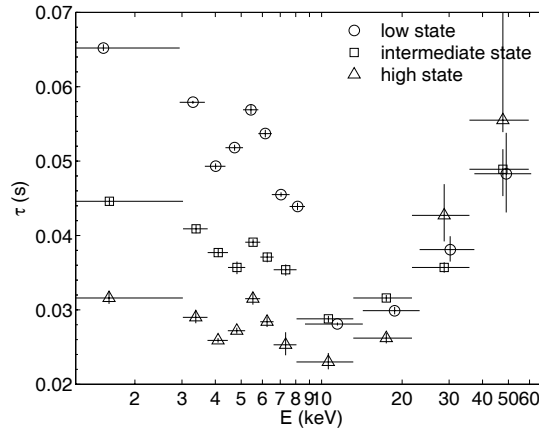


Fig. 5 Shot cutoff timescales versus energy in three states of Cyg X-1.

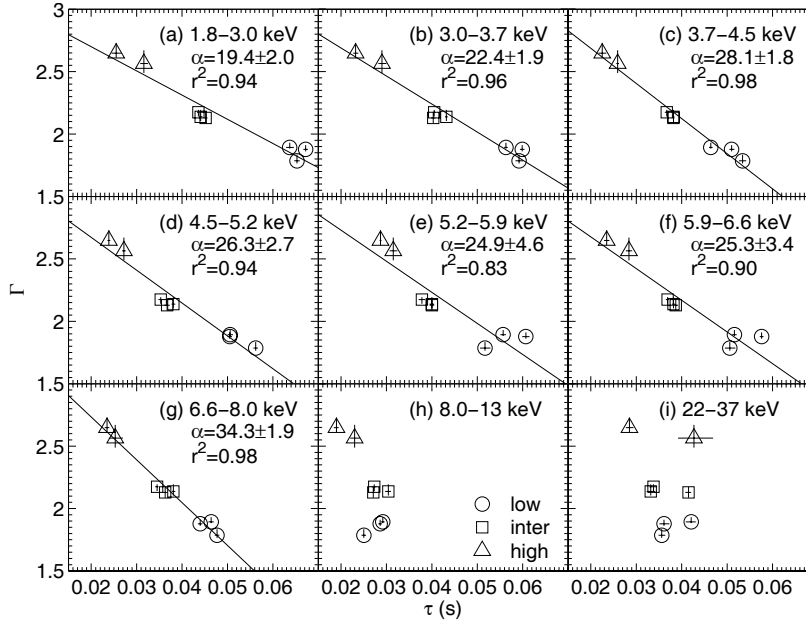


Fig. 6 Photon index versus shot cutoff timescale of Cyg X-1. The solid line is the best-fitted line labelled with the slope, standard error and correlation coefficient.

larger than the “turning point” in panels (h) and (i), there is no correlation between τ and Γ . Also in the Fe $K\alpha$ band in panels (e) and (f), the correlation at low state is somewhat weak. The best-fitted line slope α at the low energy bands seems to increase with energy increasing except in the Fe line band.

Because the “turning point” relates to the innermost region of the accretion disk, its timescale is connected with the truncation radius. From the results in Fig. 5, we find the ratio of truncation radius between low and high states is 1.14, which is conflicted with ADAF model by

Esin et al. (1998), marginally consistent with the reversal disk model by Zhang et al. (1997) and the smoothly matched ADAF-standard disk model by Lu et al. (2004), and highly consistent with the ionization model by Young et al. (2001).

We make Monte-Carlo simulations of the extended corona model (Kazanas, Hua & Titarchuk 1997) to compare with our results at the ascending part. In this model, the corona consists of an uniform-density inner core and a r^{-1} -density outer shell. The best-fitted inner core radius R_c is 11, 7 and 30 R_s , and the inner core density ρ_c is 2.0, 1.9 and 0.3 10^{16} cm^{-3} for the low, intermediate and high state, respectively. Our results indicate that in the low state, the corona is smaller and denser than the high state; the corona configuration in the low and intermediate state is similar. This conclusion contradicts the unified accretion model of Esin, McClintock & Narayan (1997). We would like to mention that the uniform-density corona model (e.g., Payne 1980; Titarchuk 1994) provides much worse fit to our results compared to the extended corona model.

5 NARROW AND BROAD IRON $K\alpha$ LINES

From a large number of shot cutoff timescales versus energy, two typical instances, one in the intermediate state and the other in a low state, are selected and shown in Fig. 7. The one in the intermediate state has a broad Fe peak and the other in the low state contains both broad and narrow Fe lines. Both broad and narrow lines present timescale-broadening. The timescale-broadening for broad line is interpreted as light bending (Fabian & Vaughan 2003; Miniutti et al. 2004). The timescale-broadening for the narrow line is probably caused by light-crossing; the Fe line reflection region can be inferred to be at radius $\leq 100R_s$ in our results.

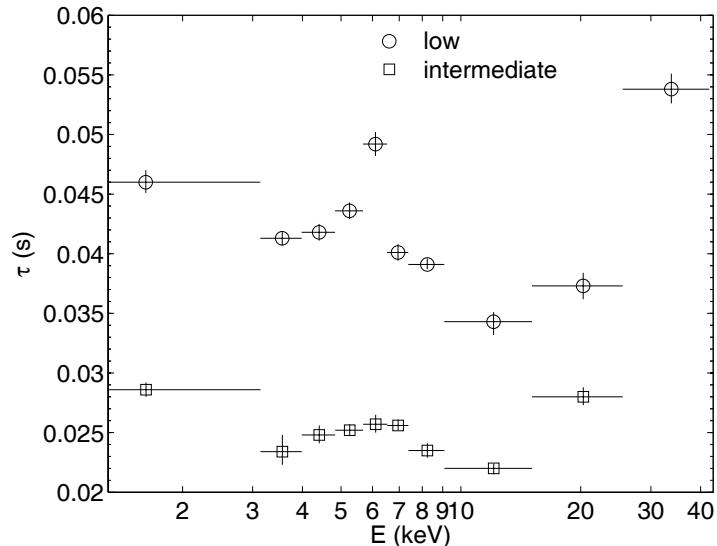


Fig. 7 Shot cutoff timescales versus energy in two observations of Cyg X-1. The intermediate state contains a broad Fe $K\alpha$ line. The low state contains a narrow line above a weak broad line.

References

- Esin A. A., Narayan R., Cui W., Grove J. E., Zhang S. N., 1998, *ApJ*, 505, 854
Li T. P., 2001, *Chin. J. Astron. Astrophys.*, 1, 313 (astro-ph/0109468)
Li T. P., Muraki Y., 2002, *ApJ*, 578, 374
Sunyaev, R., & Revnivtsev, M. 2000, *A&A*, 358, 617
Tanaka Y., Lewin W. H. G., 1995, in *X-Ray Binaries*, ed. W. H. G. Lewin, J. van Paradijs, E. P. J. Heuvel, Cambridge: Cambridge Univ. Press, 126
Esin A. A., McClintock J. E., Narayan R., 1997, *ApJ*, 489, 865
Fabian A. C., Vaughan S., 2003, *MNRAS*, 340, L28
Feng H., Li T. P., Zhang S. N., 2004, *ApJ*, 606, 424
Feng H., Zhang S. N., Li T. P., 2004, *ApJ*, 612, L45
Kazanas D., Hua X. M., Titarchuk L., 1997, *ApJ*, 480, 735
Lu J. F., Lin Y. Q., Gu W. M., 2004, *ApJ*, 602, L37
McClintock J. E., Remillard R. A., 2004, *Black Hole Binaries*, eds. W. H. G. Lewin and M. van der Klis, Cambridge Univ. Press
Miniutti G., Fabian A. C., Goyder R., Lasenby A. N., 2004, *MNRAS*, 344, L22
Payne D. G., 1980, *ApJ*, 237, 951
Poutanen J., Fabian A. C., 1999, *MNRAS*, 306, L31
Titarchuk L., 1994, *ApJ*, 434, 570
Young A. J., Fabian A. C., Ross R. R., Tanaka Y., 2001, *MNRAS*, 325, 1045
Zhang S. N., Cui W., Chen W., 1997, *ApJ*, 482, L155